Supporting Information

The Catalytic Investigation of CO_2 Chemical Fixation and Knoevenagel Condensation Reaction for a Tm^{III}-Organic Framework

Tao Zhang,[a,b] Zhengguo Zhang,[a] Hongtai Chen,[a] Xiutang Zhang[a,*] and Qiaoling Li[a,*]

[a] *North University of China, Taiyuan 030051, People's Republic of China. E-mail: xiutangzhang@163.com;*
[b] *Taiyuan Institute of Technology, Taiyuan 030008, People's Republic of China.*

Contents

X-Ray Crystallography.

Table S1. Crystallographic data and refinement parameters of NUC-28.

Table S2. Selected bond lengths and angles of NUC-28.

Table S3. CO_2 cycloaddition reaction with various catalyst.

Table S4. Comparison of the catalytic performance of NUC-28 catalyst with selected previously reported MOFs.

Table S5. The molecular sizes of various epoxides.

Table S6. Comparison of the Knoevenagel condensation catalytic performance of NUC-28 catalyst with selected previously reported MOFs.

Table S7. The molecular sizes of various benzaldehyde derivatives.

Figure S1. The $[Tm_2(CO_2)_8(OH_2)_2]_n$ chainlike cluster (a); the coordination mode of $BDCP^{5-}$ ligand of NUC-28 (b); the novel 3,4,5-connected network with the Schläfli symbol of $\{3.6^4.7\}_4\{3^2.6^2.7^2\}$ (c).

Figure S2. The IR spectrum of NUC-28.

Figure S3. TGA Curve of as-synthesized (black) and activated (red) sample of NUC-28.

Figure S4. PXRD patterns of NUC-28 under water treatment.

Figure S5. PXRD pattern after activation.

Q_{st} Calculation.

Figure S6. N_2 absorption and desorption isotherms of NUC-28 at 77 K (Insert: the pore size distribution).

Figure S7. The CO_2 sorption performance of NUC-28 at 273K and 298K.

Figure S8. CO_2 adsorption heat calculated by the virial equation of NUC-28.

Figure S9-S13. The ^1H NMR spectrums of cycloaddition reaction products.

Figure S14. The PXRD pattern of NUC-28 after recycled cycloaddition reaction.

Figure S15. The IR spectrum of NUC-28 after recycled cycloaddition reaction.

Figure S16. The FE-SEM Image of NUC-28 after recycled cycloaddition reaction.

Figure S17. The recycled cycloaddition reaction of CO_2 with styrene oxide.

Figure S18-23. The ^1H NMR spectrums of Knoevenagel condensation reaction products

Figure S24. The recycled Knoevenagel reaction using NUC-28 as catalyst.

Figure S25. The PXRD pattern of NUC-28 after recycled Knoevenagel reaction.

Figure S26. The IR spectrum of NUC-28 after recycled Knoevenagel reaction.

Figure S27. The FE-SEM Image spectrum of NUC-28 after recycled Knoevenagel reaction.

Experimental Section

Materials and General Methods

2, 6-bis(2, 4-dicarboxylphenyl)-4-(4-carboxylphenyl) pyridine (H_5BDCP) is offered by Jinan Henghua Sci. & Tec. Co. Ltd without any further refinement. The infrared (IR) spectrum is measured by TENSOR27 spectrometer in the range of 600-4000 cm^{-1}. Thermogravimetric analysis (TGA) is carried out by a TG-209F3 thermal analyzer at a heating rate of 10 °C /min under Ar stream. The powder X-ray (PXRD) diffraction analyses of the frameworks are measured on a Rigaku Smartlab (9 kW) diffractometer with Cu-Kα radiation at room temperature, and the scanning speed is 10°/min. The micro-structure of the frameworks was observed by JSM-7200F FE-SEM and the accelerating voltage is 10kV. The cryogenic N_2 adsorption and adsorption-desorption isotherms of CO_2 at 273K and 298K are measured on an ASAP 2020 Plus instrument.

Preparation of NUC-28

A homogenous solution of Tm_2O_3 (0.03 g, 0.04 mmol), H_5BDCP (0.034 g, 0.06 mmol), 8 mL DMF, 4 mL HNO_3 (1.8 M), 1mL stannous chloride solution (0.1mmol/L), and 1mL calcium chloride solution (0.1mmol/L) in 25 mL autoclave was heated at 130 °C for 2 days and then gradually cooled to room temperature. Yellowish crystals of **NUC-28** were collected by filtration and washed by DMF/H_2O. (Yield: 81 % based on H_5BDCP). Anal. Calcd. for **NUC-28** ($C_{68}H_{62}N_7O_{32}Tm_3$): C, 40.90(%); H, 3.10 (%); N, 4.91(%). Found: C, 41.12(%); H, 3.06(%); N, 4.94(%). As shown in Figure S2, IR (KBr pellet, cm^{-1}): 3425 (vs), 2935(w), 1660 (vs), 1398 (vs), 1250 (w), 1106 (w), 840 (w), 791 (s), 701(w), 661(w).

X-Ray Crystallography

The diffraction intensity data for **NUC-28** was obtained at 296(2) K using a Bruker Smart-APEX II CCD area detector (Mo-Kα radiation, λ = 0.071073 nm) with graphite-monochromated radiation. The reflection data were also corrected for empirical absorption corrections and Lorentz and polarization effects. The structures were solved by direct methods and refined by full-matrix least-squares using the SHELXL package. All non-hydrogen atoms were refined anisotropically. Hydrogen atoms except those on water molecules were generated geometrically with fixed isotropic thermal parameters, and included in the structure factor calculations. The block of SQUEEZE in PLATON was employed to eliminate the highly disordered solvent molecular. The solvent content of **NUC-28** was determined by the thermogravimetric analysis (Figure S3) and elemental analysis. Crystallographic data and refinement parameter for **NUC-28** are given in Table S1. Selected bond lengths and angles for **NUC-28** are listed in Table S2. Further details on the crystal structure investigations may be obtained from the Cambridge Crystallographic Data Centre, with the depository number CCDC-2052343 for **NUC-28**.

Table S1. Crystallographic data and refinement parameters of NUC-28.

Complex	**NUC-28**
Formula	$C_{56}H_{30}N_3O_{26}Tm_3$
M_r	1667.62
Crystal system	triclinic
Space group	*P-1*
a (Å)	9.2560(8)
b (Å)	15.8648(15)
c (Å)	28.250(3)
α (°)	96.574(4)
β (°)	90.095(3)
γ (°)	104.682(3)
V(Å^3)	3984.5(6)
Z	2
Dcalcd(g·cm^{-3})	1.390
μ(mm^{-1})	3.376
GOF	1.099
R_1 [I＞2σ(I)]^a	0.0437
wR_2 [I＞2σ(I)]^b	0.1162
R_1^{a} (all data)	0.0517
wR_2^{b} (all data)	0.1197
R_{int}	0.0620

$^a R_1 = \sum ||F_o|-|F_c|| / \sum |F_o|$. $^b wR_2 = [\sum w(|F_o|^2-|F_c|^2)/\sum [w(F_o^2)^2]]^{1/2}$

Table S2. Selected bond lengths and angles of NUC-28.

O1W-Tm1	2.329(4)	O1-Tm1	2.240(4)	O2-Tm2#4	2.244(4)
O3-Tm1	2.240(4)	O4-Tm2#4	2.229(4)	O5-Tm3#2	2.211(6)
O8-Tm3#4	2.241(4)	O9-Tm1#1	2.378(4)	O10-Tm1#1	2.349(4)
O11-Tm1	2.234(4)	O12-Tm2	2.210(4)	O13-Tm1	2.226(4)
O14-Tm2	2.249(4)	O15-Tm3	2.237(4)	O17-Tm2#	2.371(4)
O18-Tm2#3	2.360(4)	O19-Tm3#2	2.361(5)	O20-Tm3#2	2.426(5)
O2W-Tm2	2.341(4)	O22-Tm3	2.409(7)	Tm3-O23	2.431(7)
Tm3-O3W	2.367(7)				
O1W-Tm1-O9#1	150.24(16)	O1W-Tm1-O10#1	150.49(14)	O1-Tm1-O1W	84.67(15)
O1-Tm1-O9#1	74.11(14)	O1-Tm1-O10#1	124.82(14)	O3-Tm1-O1W	92.26(15)
O3-Tm1-O1	82.94(15)	O3-Tm1-O9#1	105.27(16)	O3-Tm1-O10#1	90.66(16)
O10#1-Tm1-O9#1	54.94(14)	O11-Tm1-O1W	78.43(14)	O11-Tm1-O1	108.56(16)
O11-Tm1-O3	164.18(15)	O11-Tm1-O9#1	88.65(15)	O11-Tm1-O10#1	91.34(15)
O13-Tm1-O1W	77.92(15)	O13-Tm1-O1	156.69(14)	O13-Tm1-O3	82.39(15)
O13-Tm1-O9#1	127.44(14)	O13-Tm1-O10#1	73.38(14)	O13-Tm1-O11	83.15(15)
O2#5-Tm2-O17#3	129.53(15)	O2#5-Tm2-O18#3	75.00(14)	O2#5-Tm2-O2W	79.06(14)
O4#5-Tm2-O25	86.48(15)	O4#5-Tm2-O14	106.47(15)	O4#5-Tm2-O17#3	85.07(15)
O4#5-Tm2-O18#3	88.88(15)	O4#5-Tm2-O2W	78.83(14)	O12-Tm2-O2#5	82.83(15)
O12-Tm2-O4#5	168.81(14)	O12-Tm2-O14	82.49(15)	O12-Tm2-O17#3	104.30(16)
O12-Tm2-O18#3	91.52(16)	O12-Tm2-O2W	95.85(15)	O14-Tm2-O17#3	72.69(14)
O14-Tm2-O18#3	124.18(13)	O14-Tm2-O2W	83.74(14)	O18#3-Tm2-O17#3	55.19(13)
O2W-Tm2-O17#3	146.32(15)	O2W-Tm2-O18#3	151.90(13)	O5#6-Tm3-O8#5	100.74(19)
O5#6-Tm3-O15	79.67(18)	O5#6-Tm3-O19#6	86.8(2)	O5#6-Tm3-O20#6	83.6(2)
O5#6-Tm3-O22	78.2(3)	O5#6-Tm3-O23	133.6(2)	O5#6-Tm3-O3W	158.8(2)
O8#5-Tm3-O19#6	147.60(17)	O85-Tm3-O206	157.66(17)	O8#5-Tm3-O22	77.5(2)
O8#5-Tm3-O23	79.8(2)	O8#5-Tm3-O3W	86.4(2)	O15-Tm3-O85	81.63(16)
O15-Tm3-O19#6	130.77(17)	O15-Tm3-O20#6	77.60(16)	O15-Tm3-O22	145.9(3)
O15-Tm3-O23	144.4(2)	O15-Tm3-O3W	81.7(2)	O19#6-Tm3-O20#6	53.84(17)
O19#6-Tm3-O22	73.3(2)	O19#6-Tm3-O23	72.6(2)	O19#6-Tm3-O3W	97.9(2)
O20#6-Tm3-O23	113.2(3)	O22-Tm3-O20#6	124.7(2)	O22-Tm3-O23	56.3(3)

O3W-Tm3-O20#6	82.6(3)	O3W-Tm3-O22	123.0(3)	O3W-Tm3-O23	67.2(3)
#1: -X,1-Y,1-Z; #2: 1+X,1+Y,+Z; #3: -1-X,1-Y,-Z; #4: 1+X,+Y,+Z; #5: -1+X,+Y,+Z; #6: -1+X,-1+Y,+Z					

Table S3. CO_2 cycloaddition reaction with various catalyst.[a]

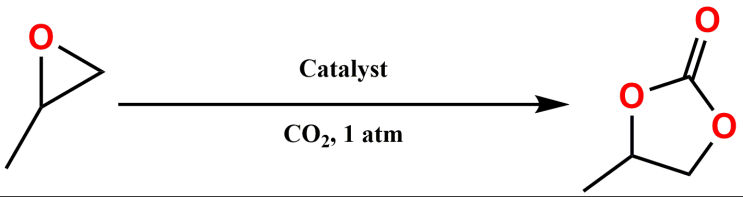

Entry	Catalyst	Epoxide	product	Yield (%)[b]
1	$Tm(NO_3)_3$	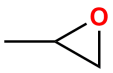	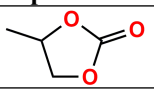	38
2	$Tm(NO_3)_3$+*n*-Bu_4NBr	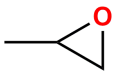	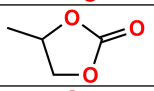	57
3	H_5DBCP	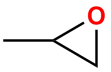	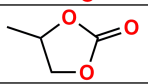	22
4	H_5DBCP+*n*-Bu_4NBr	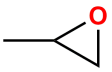	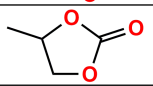	24
5	-	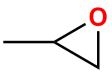	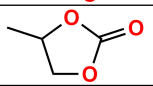	6

[a]Reaction conditions: Substrates (20 mmol), Bu_4NBr (5 mol %), **NUC-28** (0.5 mol %, based on the Tm(III) center), CO_2 (1 atm), 60 °C, 6 h. [b]Determined by GC/MS with n-dodecane as the internal standard.

Table S4. Comparison of the catalytic performance of NUC-28 catalyst with selected previously reported MOFs.

MOF	Catalyst (mol %)	Temperature (℃)	Pressure (MPa)	Time (h)	Yield (%)	Ref.
$[La_2(HL)_2(H_2L)(NO_3)(CH_3OH)(H_2O)]$	0.05	120	0.8	2	94	S1
NH_2-MIL-101(Al)	0.17	120	1.8	6	95	S2
Hf-Nu-1000	4.0	55	0.1	12	95	S3
Cr-MIL-101	1.2	RT	0.8	24	82	S4
Sm/Gd-BTB	1.0	80	0.1	15	100	S5
Tb-BDC	0.05	60	1.0	12	89	S6
Tb-NDC	0.05	60	1.0	12	87	S6
$\{[TbZn(BPDC)_2(\mu_2\text{-}H_2O)Cl(H_2O)_3]\cdot 5H_2O\cdot 0.5DMA\}_n$	1.0	70	0.1	12	>99	S7
NUC-28	2.5	60	0.1	6	99	This work

Table S5. The molecular sizes of various epoxides.

Entry	Epoxides	Molecular Size[a] (Å3)
1	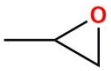	4.843*6.355*5.027
2	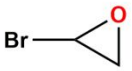	4.773*4.982*6.484
3	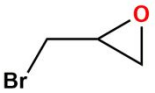	5.907*7.545*5.159
4	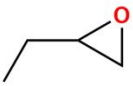	7.305*5.167*5.470
5	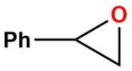	7.186*4.899*9.403

Table S6. Comparison of the Knoevenagel condensation catalytic performance of NUC-28 catalyst with selected previously reported MOFs.

MOFs	Solvent	Temperature (°C)	Time (h)	Yield (%)	Ref.
UiO-66-NH_2	Ethanol	80	2	94	S8
UPC-102-Zr	CH_2Cl_2	RT	5	88.9	S9
ZIF8-A61-SO_3H	H_2O	90	4	98	S10
UiO-66-NH-RNH_2	Toluene	RT	2	97	S11
$[Zn_2(L)(H_2O)_2]\cdot(DMF)_5\cdot(H_2O)_4]$	CH_2Cl_2	RT	2	90	S12
Yb-BDC-NH_2	DMSO-d_6	50	24	97	S13
Dy-BDC-NH_2	DMSO-d_6	50	24	82	S13
Sm-BDC-NH_2	DMSO-d_6	50	24	76	S13
$\{[Eu(TATMA)(H_2O)\cdot 2H_2O\}_n$	Toluene	80	3	98	S14
NUC-28	Ethanol	50	18	97	This work

Table S7. The molecular sizes of various benzaldehyde derivatives.

Enrty	Substrate	Molecular Size[a] (Å3)
1	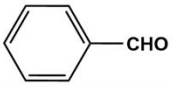	7.133*8.656*2.400
2	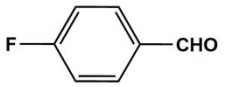	6.996*9.137*2.900
3	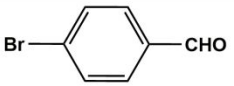	6.897*10.064*2.456
4	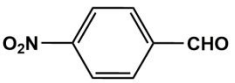	6.929*9.857*2.400
5	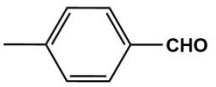	6.999*9.477*4.218
6	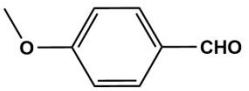	10.945*6.996*4.244

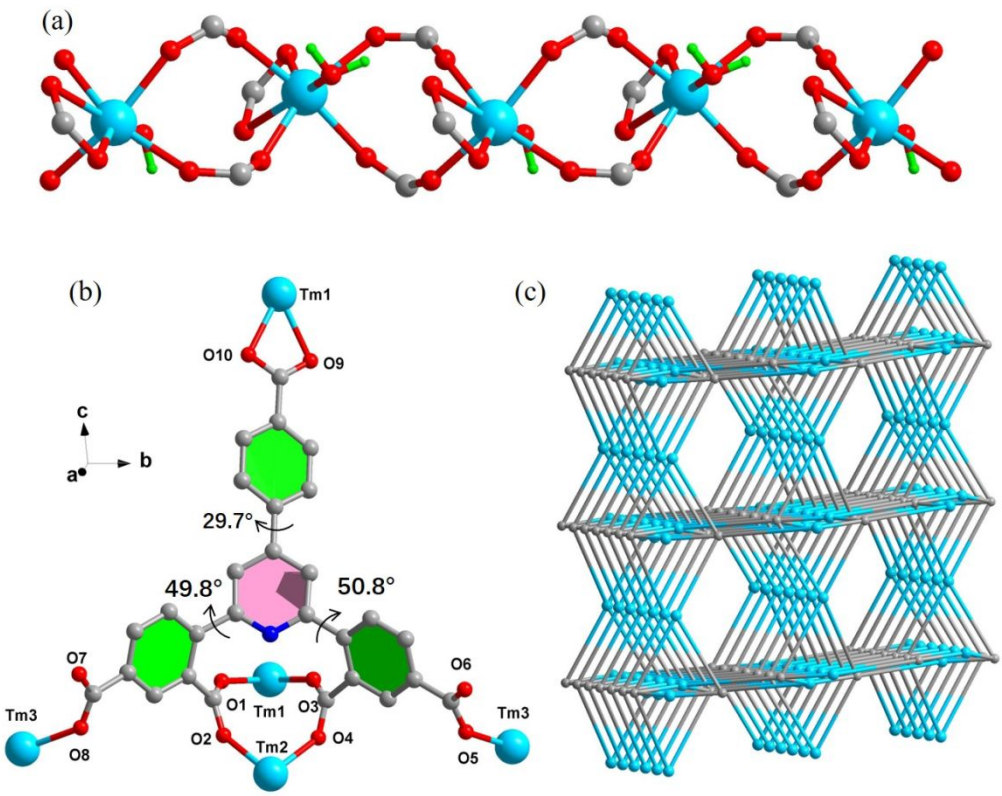

Figure S1. The $[Tm_2(CO_2)_8(OH_2)_2]_n$ chainlike cluster (a); the coordination mode of $BDCP^{5-}$ ligand of NUC-28 (b); the novel 3,4,5-connected network with the Schläfli symbol of $\{3.6^4.7\}_4\{3^2.6^2.7^2\}$ (c).

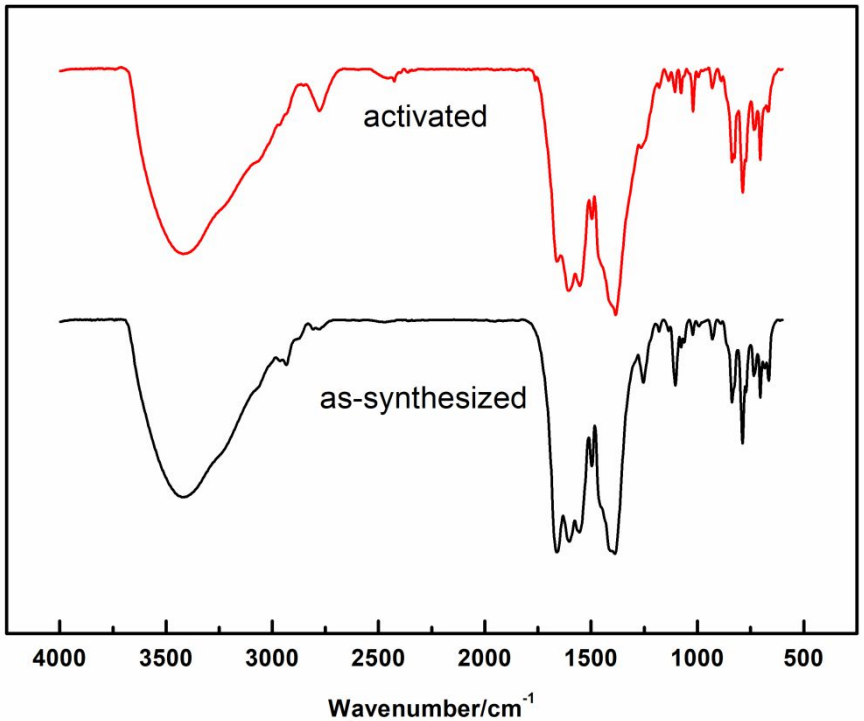

Figure S2. The IR spectrum of NUC-28.

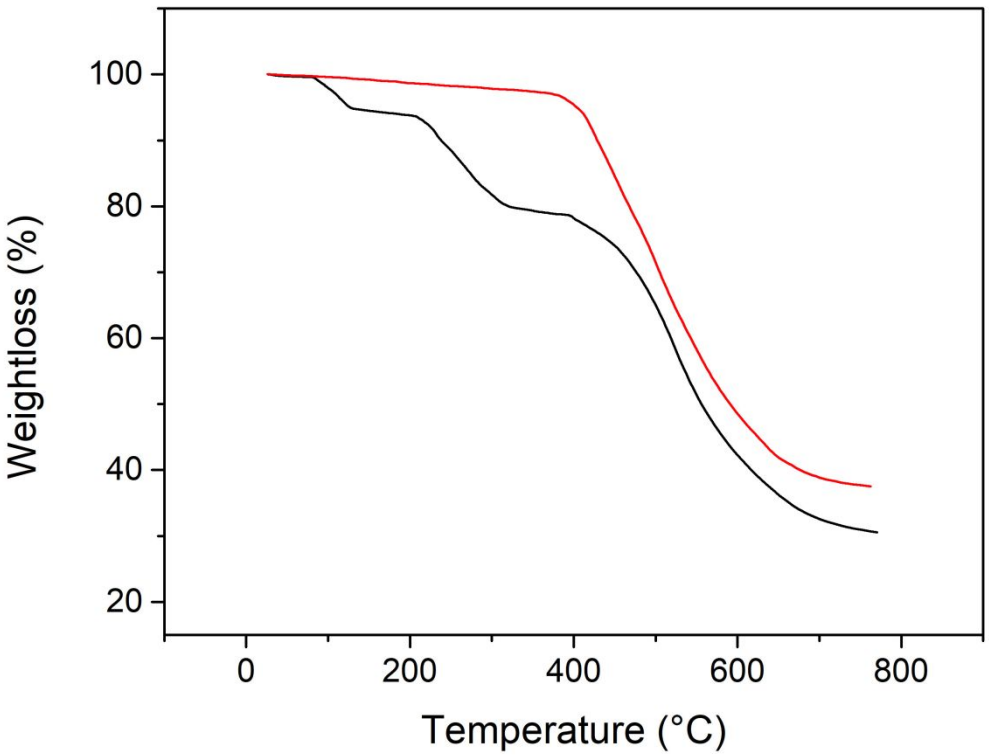

Figure S3. TGA Curve of as-synthesized (black) and activated (red) sample of NUC-28.

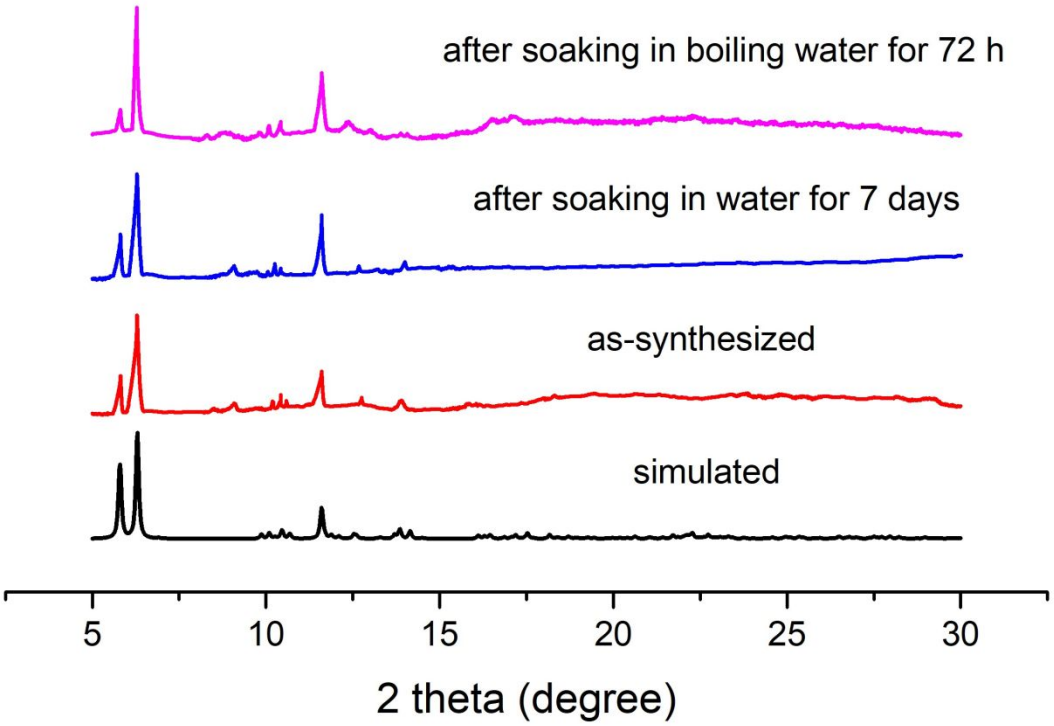

Figure S4. PXRD patterns of NUC-28 under water treatment.

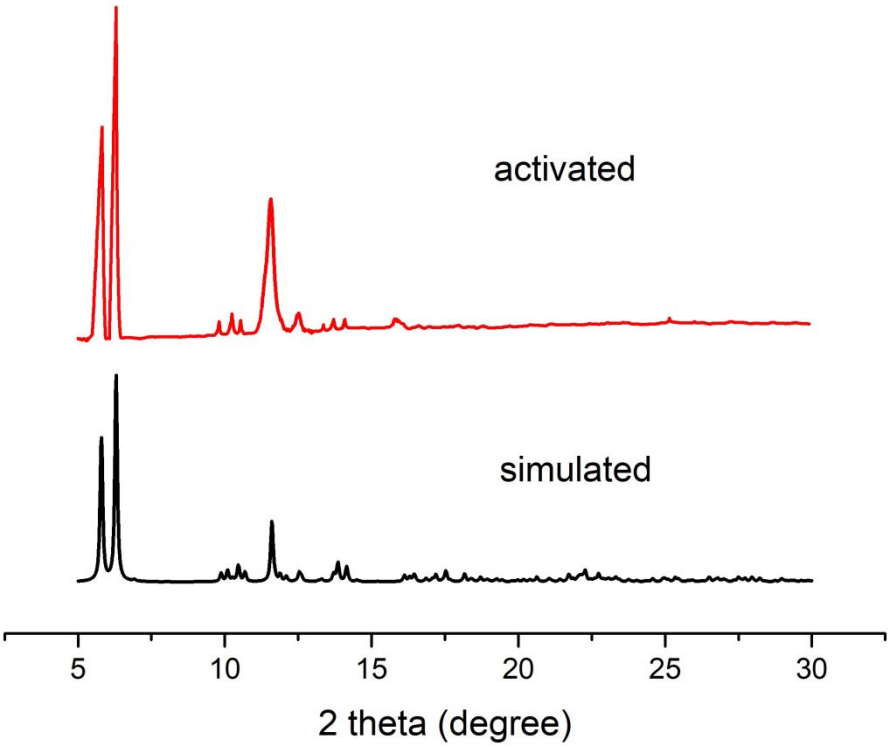

Figure S5. PXRD pattern after activation.

Q_{st} Calculation.

The Q_{st} value is a parameter that describes the average enthalpy of adsorption for an adsorbing gas mole Cole at a specific surface coverage and is usually evaluated using two or more adsorption isotherms collected at similar temperatures. The zero-coverage isosteric heat of adsorption is evaluated by first fitting the temperature-dependent isotherm data to a virial-type expression, which can be written as:

$$lnP = lnN + \frac{1}{T}\sum_{i=0}^{m} a_i N^i + \sum_{i=0}^{n} b_i N^i \qquad \text{(Equation 1)}$$

$$Q_{st} = -R\sum_{i=0}^{m} a_i N^i \qquad \text{(Equation 2)}$$

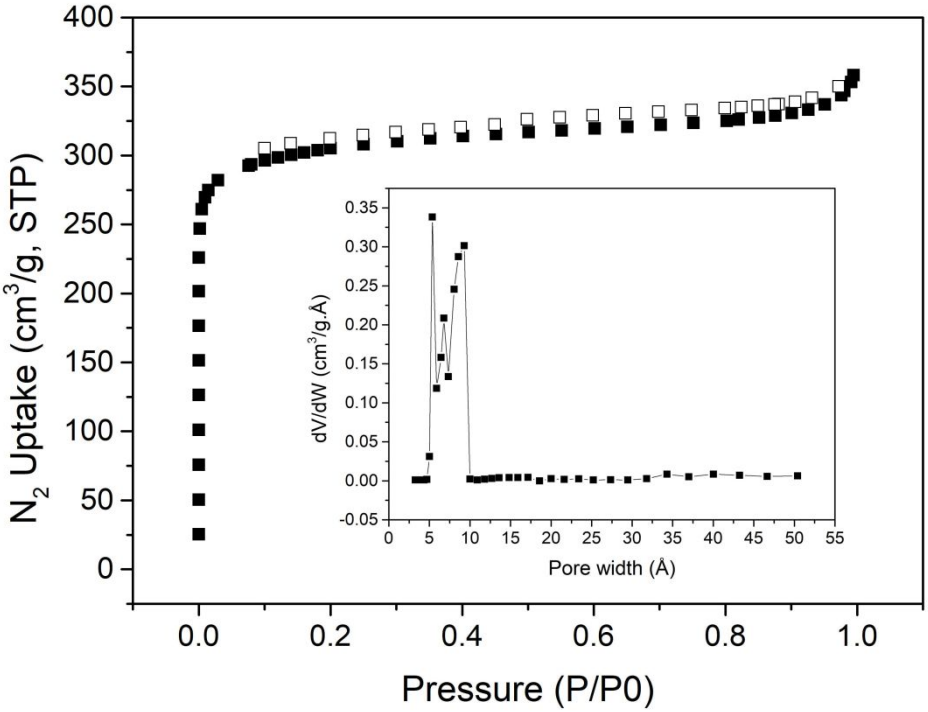

Figure S6. N_2 absorption and desorption isotherms of NUC-28 at 77 K (Insert: the pore size distribution).

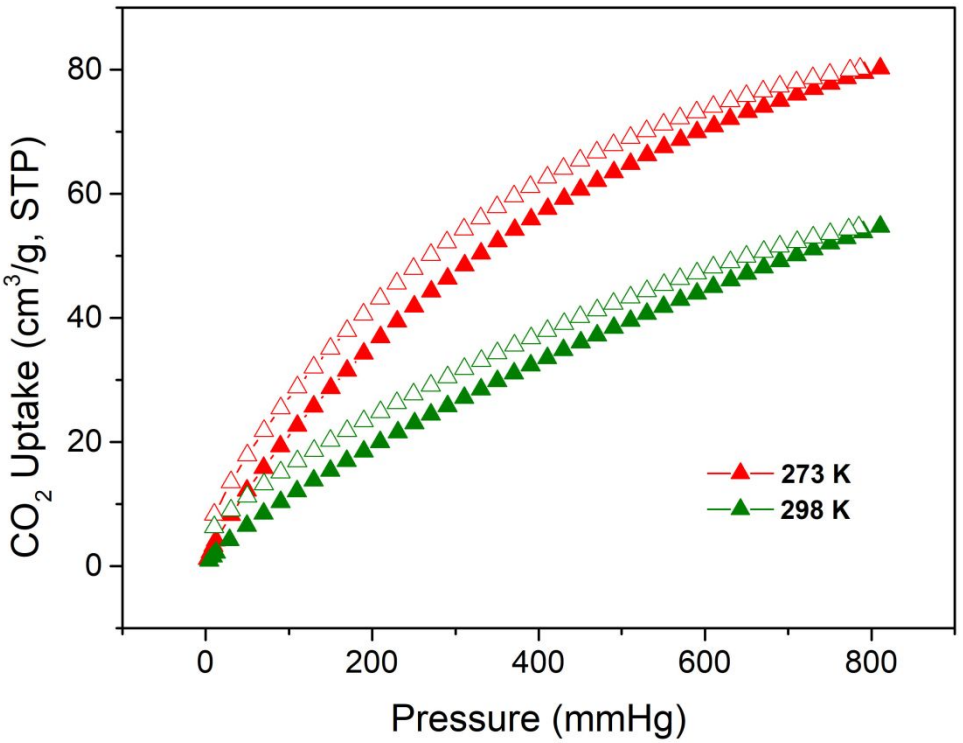

Figure S7. The CO_2 sorption performance of NUC-28 at 273K and 298K.

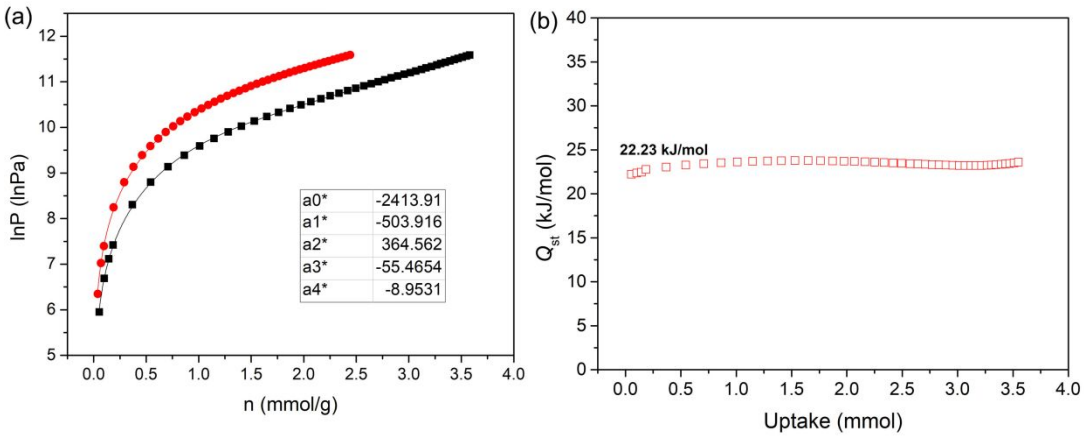

Figure S8. The fitting parameters of CO_2 adsorption heat(a); CO_2 adsorption heat calculated by the virial equation of NUC-28 (b).

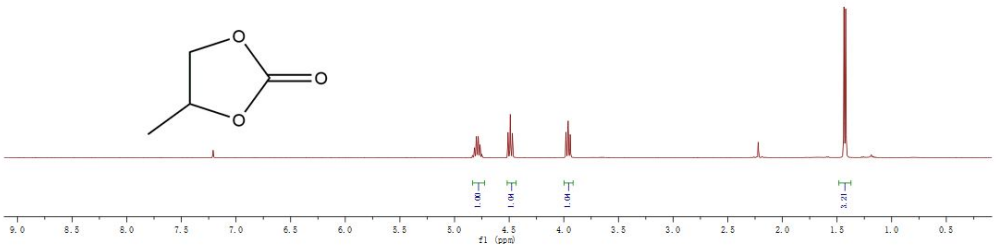

Figure S9. The ^{1}H NMR spectrum of 4-methyl-1,3-dioxolan-2-one (Table 2, entry 1).

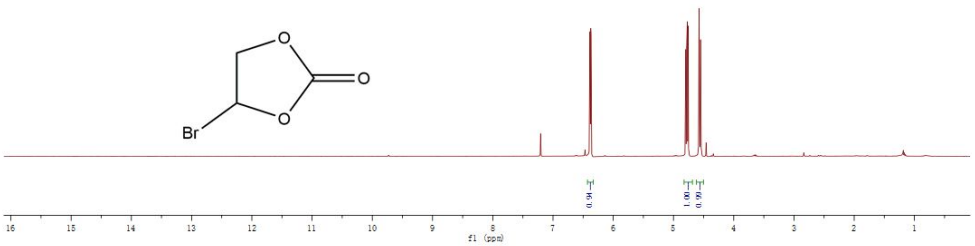

Figure S10. The ^{1}H NMR spectrum of 4-bromomethyl-1,3-dioxolan-2-one (Table 2, entry 2).

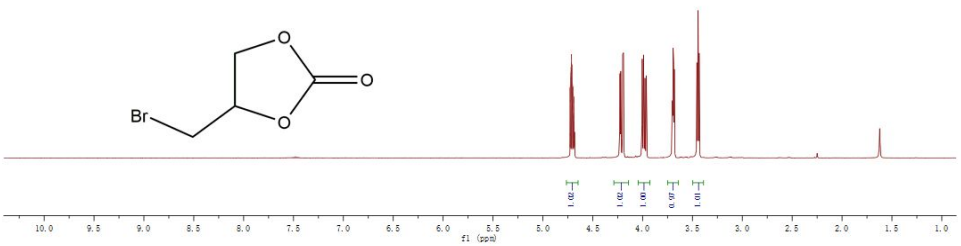

Figure S11. The ^{1}H NMR spectrum of 4-(bromomethyl)-1,3-dioxolan-2-one (Table 2, entry 3).

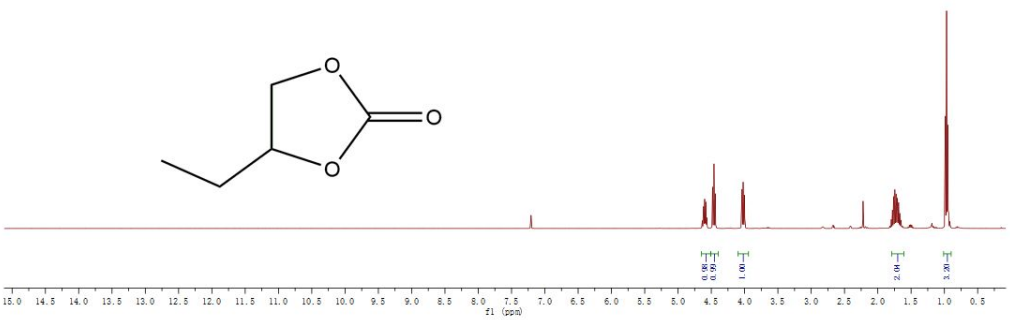

Figure S12. The ^{1}H NMR spectrum of 4-ethyl-1,3-dioxolan-2-one (Table 2, entry 4).

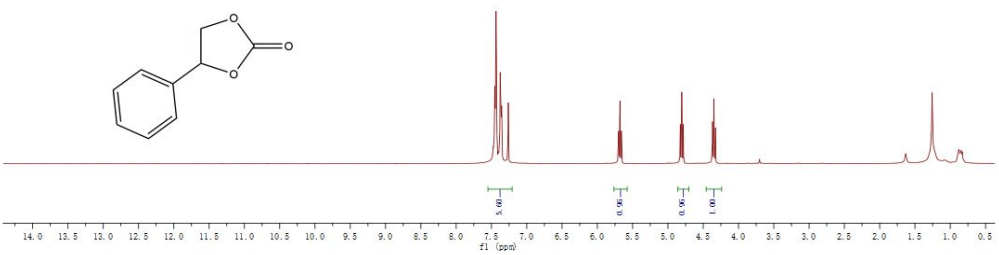

Figure S13. The ^{1}H NMR spectrum of 4-phenyl-1,3-dioxolan-2-one (Table 2, entry 5).

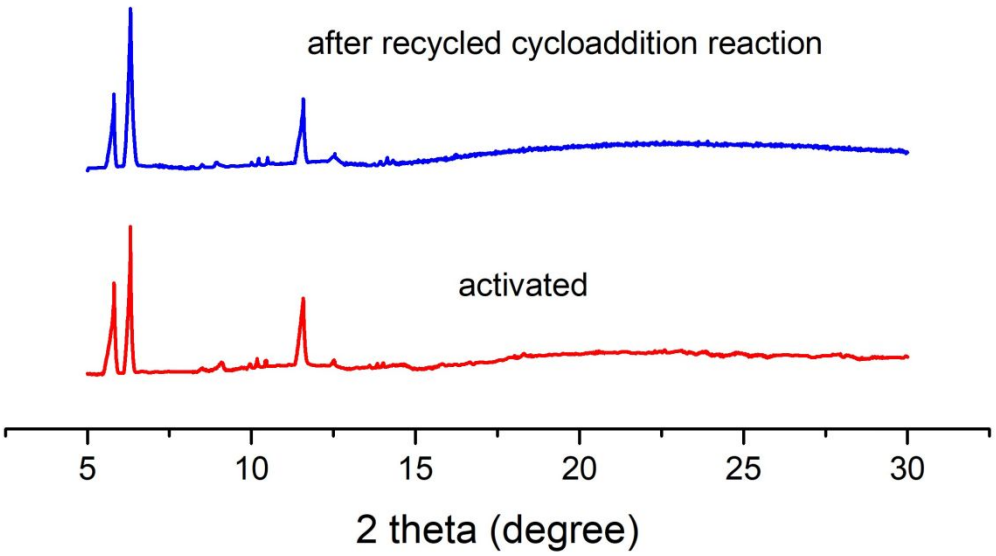

Figure S14. The PXRD pattern of NUC-28 after recycled cycloaddition reaction.

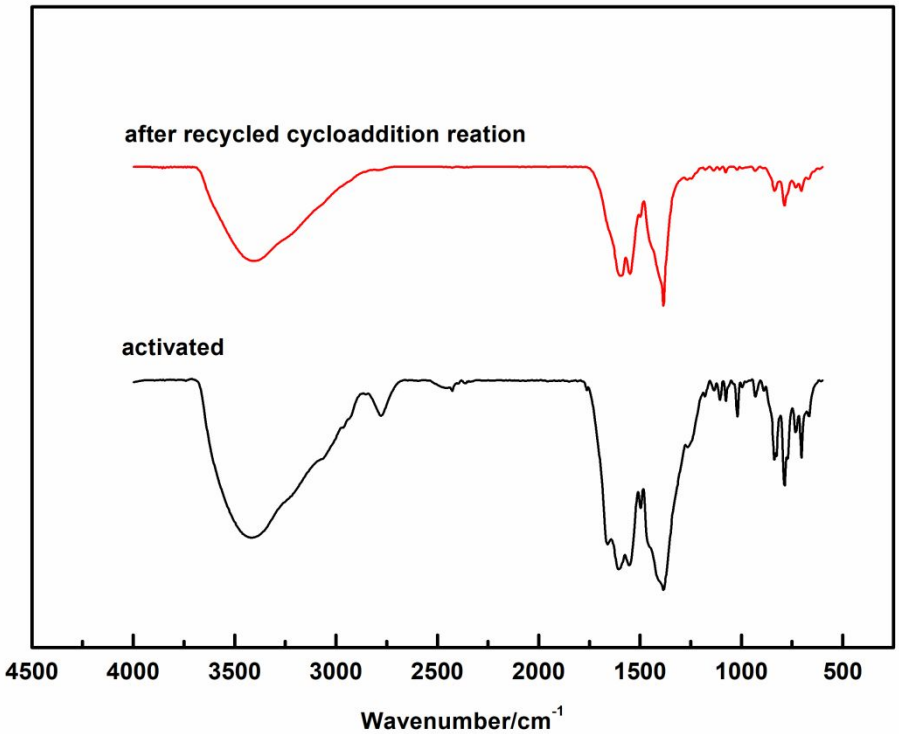

Figure S15. The IR spectrum of NUC-28 after recycled cycloaddition reaction.

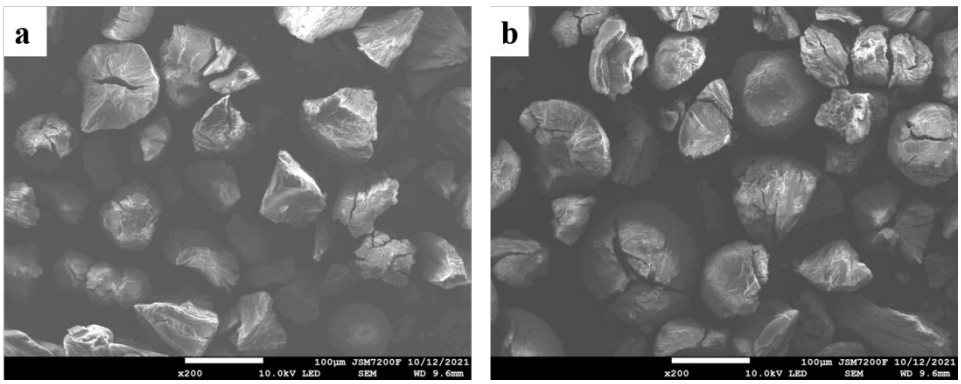

Figure S16. The FE-SEM images of NUC-28 before (a) and after (b) recycled cycloaddition reaction.

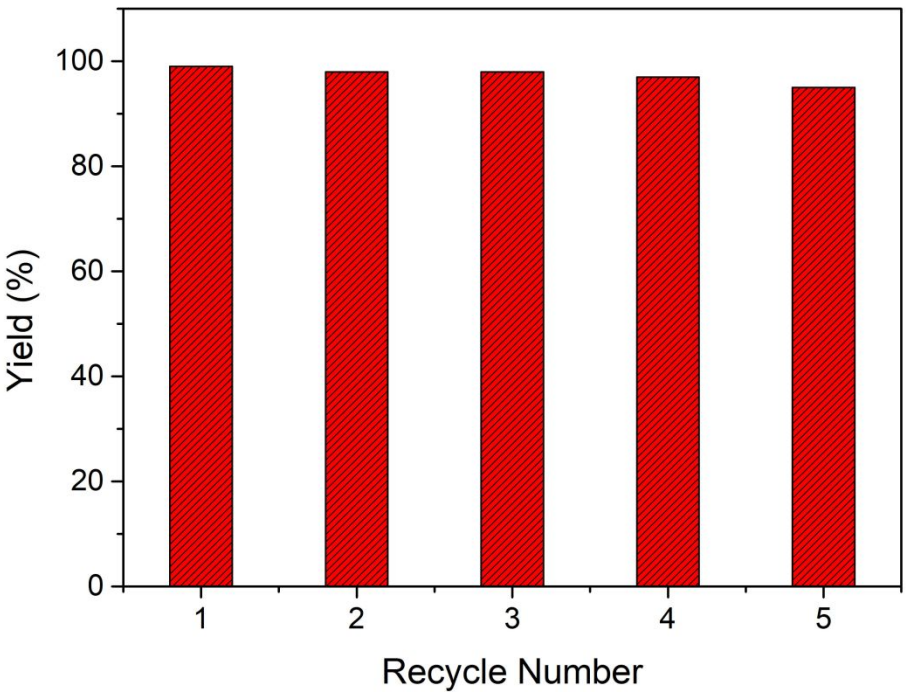

Figure S17. The recycled cycloaddition reaction of CO_2 with styrene oxide.

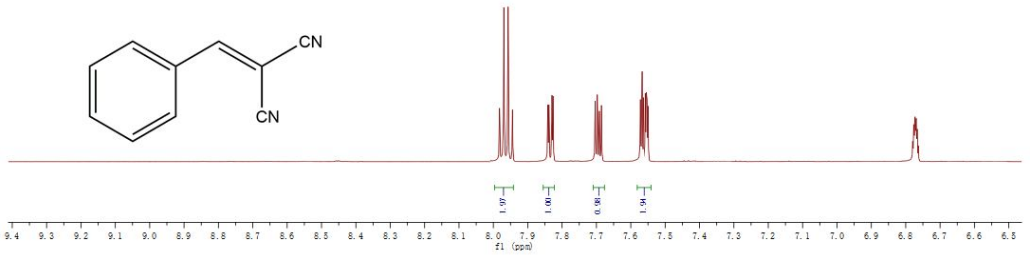

Figure S18. ^{1}H NMR spectrum of benzylidene malononitrile (Table 4, entry 1).

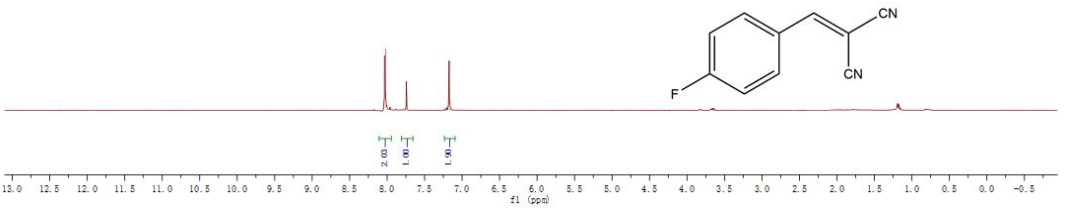

Figure S19. ^{1}H NMR spectrum of 2-(4-fluorobenzylidene)malononitrile (Table 4, entry 2).

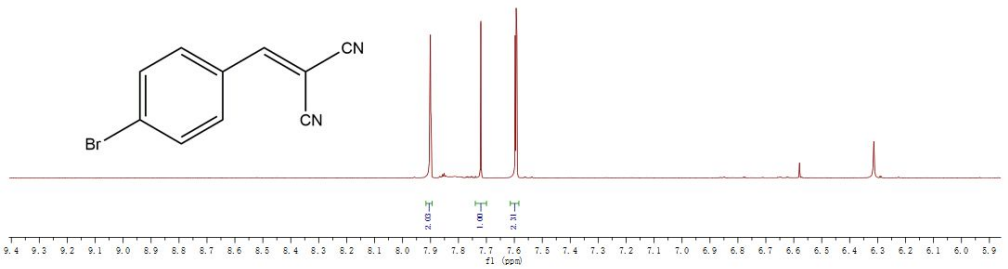

Figure S20. ^{1}H NMR spectrum of 2-(4-bromobenzylidene)malononitrile (Table 4, entry 3).

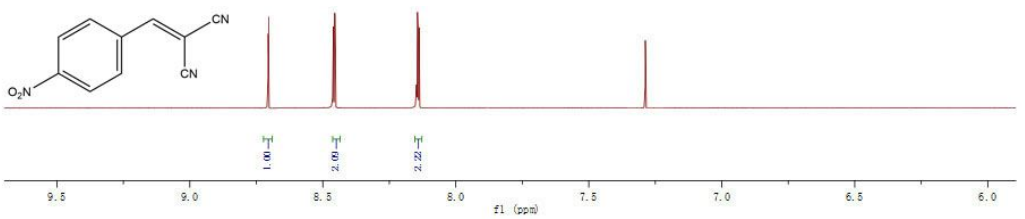

Figure S21. ^{1}H NMR spectrum of 2-(4-nitrobenzylidene)malononitrile (Table 4, entry 4).

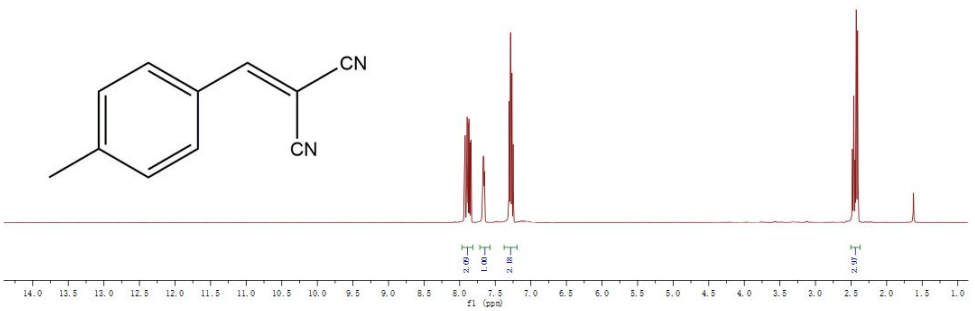

Figure S22. ^{1}H NMR spectrum of 2-(4-methylbenzylidene)malononitrile (Table 4, entry 5).

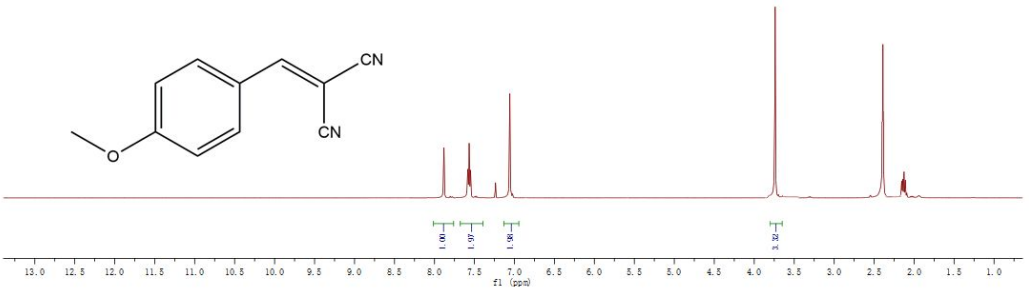

Figure S23. ^{1}H NMR spectrum of 2-(4-methoxybenzylidene)malononitrile (Table 4, entry 6).

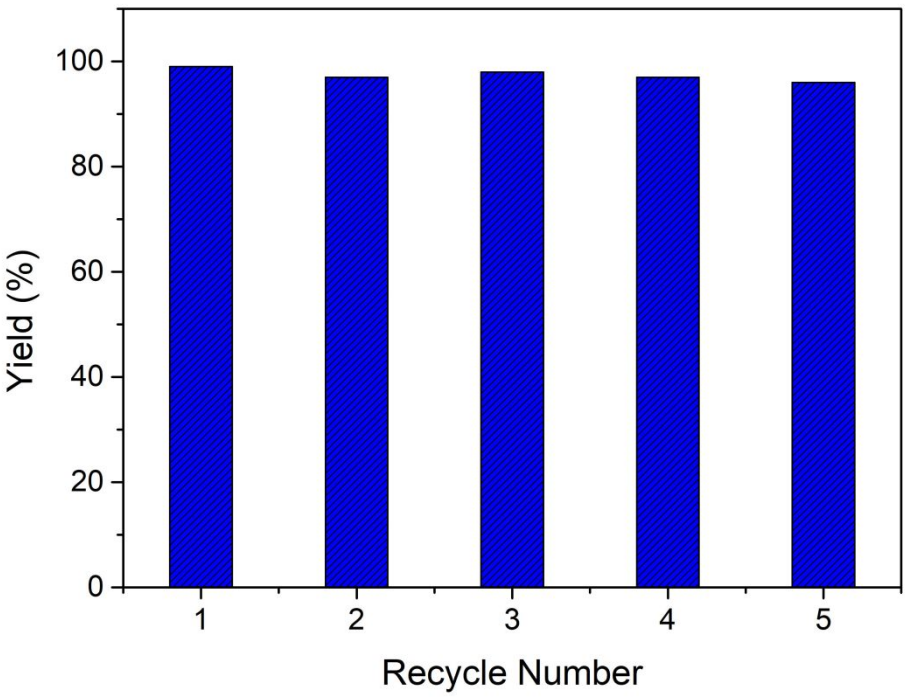

Figure S24. The recycled Knoevenagel reaction using NUC-28 as catalyst.

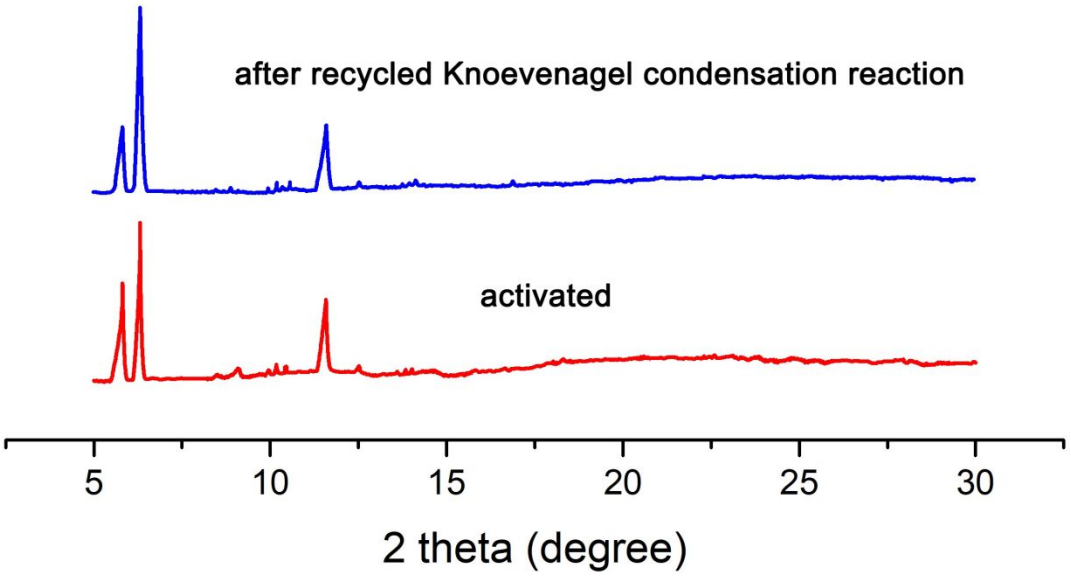

Figure S25. The PXRD pattern of NUC-28 after recycled Knoevenagel reaction.

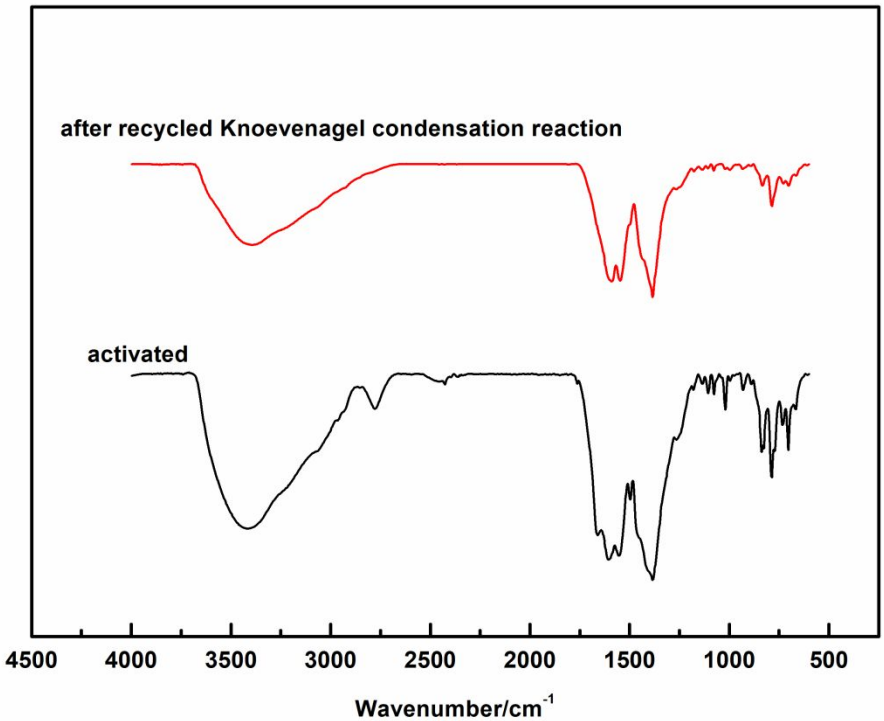

Figure S26. The IR spectrum of NUC-28 after recycled Knoevenagel reaction.

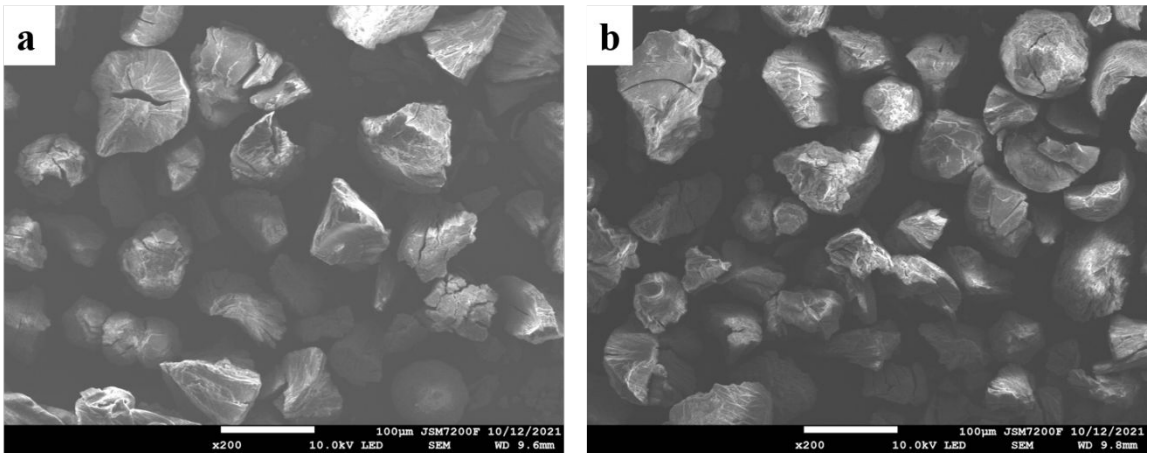

Figure S27. The FE-SEM images of NUC-28 before (a) and after (b) recycled Knoevenagel reaction.

Reference

S1. Babu, R. Roshan, R.; Kathalikkattil, A. C.; Kim, D. W.; Park D.-W. Rapid, Microwave-Assisted Synthesis of Cubic, Three-Dimensional, Highly Porous MOF-205 for Room Temperature CO_2 Fixation via Cyclic Carbonate Synthesis. *New J. Chem.,* **2021**, DOI: 10.1039/d1nj03652a.

S2. Senthilkumar, S.; Maru, M. S.; Somani, R. S.; Bajaj, H. C.; Neogi, S. Unprecedented NH_2-MIL-101(Al)/n-Bu_4NBr System as Solvent-Free Heterogeneous Catalyst for Efficient Synthesis of Cyclic Carbonates via CO_2 Cycloaddition. *Dalton Trans*. **2018**, *47*, 418−428.

S3. Beyzavi, M. H.; Klet, R. C.; Tussupbayev, S.; Borycz, J.; Vermeulen, N. A.; Cramer, C. J.; Stoddart, J. F.; Hupp, J. T.; Farha, O. K. A Hafnium-Based Metal–Organic Framework as an Efficient and Multifunctional Catalyst for Facile CO_2 Fixation and Regioselective and Enantioretentive Epoxide Activation. *J. Am. Chem. Soc.* **2014**, *136*, 15861–15864.

S4. Zalomaeva, O. V.; Chibiryaev, A. M.; Kovalenko, K. A.; Kholdeeva, O. A.; Balzhinimaev, B. S.; Fedin, V. P. Cyclic Carbonates Synthesis from Epoxides and CO_2 Over Metal−organic Framework Cr-MIL-101. *J. Catal*. **2013**, *298*, 179−185.

S5. Ugale, B.; Dhankhar, S. S.; Nagaraja C. M. Exceptionally stable and 20-connected lanthanide metal-organic frameworks (MOFs) for selective CO_2 capture and conversion to cyclic carbonates at atmospheric pressure. *Cryst. Growth Des.* **2018**, *18*, 2432–2440.

S6. Wei, N.; Zuo, R.-X.; Zhang, Y.-Y.; Han, Z.-B.; Gu, X.-J. Robust high-connected rare-earth MOFs as efficient heterogeneous catalysts for CO_2 conversion. *Chem. Commun.*, **2017**, *53*, 3224−3227.

S7. Qiao, W.-Z.; Xu, H.; Cheng, P.; Zhao B. 3d-4f Heterometal-Organic Frameworks for Efficient Capture and Conversion of CO_2. *Cryst. Growth Des.* **2017**, *17*, 3128–3133.

S8. Yang, Y.; Yao, H.-F.; Xi, F.-G.; Gao, E.-Q. Amino-Functionalized Zr(IV) Metal−Organic Framework as Bifunctional Acid−Base Catalyst for Knoevenagel Condensation. *J. Mol. Catal. A: Chem*. **2014**, *390*, 198−205.

S9.Fan, W.; Wang, X.; Xu, R.; Wang, Y.; Liu, D.; Zhang, M.; Shang, Y.; Dai, F.; Zhang, L.; Sun, D. Amino-Functionalized MOFs with High Physicochemical Stability for Efficient Gas Storage/Separation, Dye Adsorption and Catalytic Performance. *J. Mater. Chem. A* **2018**, *6*, 24486–24495.

S10. Lee, Y. R.; Do, X. H.; Hwang, S. S.; Baek, K. Y. Dual-functionalized ZIF-8 as An Efficient Acid-base Bifunctional Catalyst for the One-pot Tandem Reaction. *Catal. today* **2019**, DOI: 10.1016/j.cattod.2019.06.076.

S11. Luan, Y.; Qi, Y.; Gao, H. Y.; Andriamitantsoa, R. S.; Zheng, N. N.; Wang, G. A General Post-Synthetic Modification Approach of Amino-Tagged Metal-Organic Frameworks to Access Efficient Catalysts for the Knoevenagel Condensation Reaction. *J. Mater. Chem. A* **2015**, *3*, 17320−17331.

S12. Pal, T. K.; De, D.; Neogi, S.; Pachfule, P.; Senthilkumar, S.; Xu, Q.; Bharadwaj, P. K. Significant Gas Adsorption and Catalytic Performance by a Robust Cu^{II} −MOF Derived through Single-Crystal to Single-Crystal Transmetalation of a Thermally Less-Stable Zn^{II} −MOF. *Chem. Eur. J.* **2015**, *21*, 19064−19070.

S13. Zhang, Y.; Wang, Y.; Liu, L.; Wei, N.; Gao, M.-L.; Zhao, D.; Han, Z.-B. Robust Bifunctional Lanthanide Cluster Based Metal−Organic Frameworks (MOFs) for Tandem Deacetalization−Knoevenagel Reaction. *Inorg. Chem.*, **2018**, *57*, 2193−2198.

S14. Zhao, S. A Novel 3D MOF with Rich Lewis Basic Sites as a Base Catalysis Toward Knoevenagel Condensation Reaction. *Journal of Molecular Structure*, **2018**, *1167*, 11−15.